Metal Cluster Electrides: a new Type of Molecular Electrides with Delocalised Polyattractor Character

Ouissam El Bakouri[a], Verònica Postils[a], Marc Garcia-Borràs[a,b], Miquel Duran[a], Josep M. Luis[a], Simone Calvello[c], Alessandro Soncini[c], Eduard Matito*[,d,e], Ferran Feixas*[,a] and Miquel Solà*[,a]

[a] *Institut de Química Computacional i Catàlisi (IQCC) and Departament de Química, Universitat de Girona, C/ Maria Aurèlia Capmany 69, 17003 Girona, Catalonia, Spain. E-mail: ferran.feixas@udg.edu, miquel.sola@udg.edu*

[b] *Department of Chemistry and Biochemistry, University of California, Los Angeles, California 90095, United States.*

[c] *School of Chemistry, University of Melbourne, VIC 3010, Australia.*

[d] *Kimika Fakultatea, Euskal Herriko Unibertsitatea (UPV/EHU), and Donostia International Physics Center (DIPC), P.K. 1072, 20080 Donostia, Euskadi, Spain. E-mail: ematito@gmail.com*

[e] *Ikerbasque, Basque Foundation for Science, 48011 Bilbao, Euskadi, Spain.*

Abstract

Electrides are ionic substances that present isolated electrons. These confined electrons are topologically characterised by a quasiatom, i.e. a non-nuclear attractor (NNA) of the electron density. The electronic structure of octahedral $^4A_{1g}$ Li_6^+ and $^5A_{1g}$ Be_6 species shows that these species have a large number of NNAs. These NNAs present highly delocalised electron densities and, as a result, the chemical bonding pattern of these systems reminds that of the solid metals where metal cations are surrounded by a "sea" of delocalised valence electrons. We propose the term metal cluster electrides to refer to this new type of compounds. In this study, we establish a computational protocol to identify, characterize, and design metal cluster electrides and we elucidate the intricate bonding patterns of this particular type of species.

Introduction

A solid electride is an ionic substance in which confined electrons trapped in a cavity serve as anions.[1-2] Because of the presence of these loosely bound anionic electrons,[3] solid electrides have particular properties such as high nonlinear optical behaviour,[4-6] large magnetic susceptibility,[7] superconductivity,[8] or high reducing power.[1-2] Interestingly, some of these electrides can boost nitrogen dissociation facilitating the process of ammonia synthesis.[9-14] To date fifteen (seven inorganic and eight organic) solid electrides have been reported; eight out of these fifteen are stable at room temperature.[13, 15-19] In some other cases, the electride character is revealed only at high pressure.[20-27] *Molecular electrides*[28] are another type of electrides that have an electron (or a significant portion of an electron) that cannot be assigned to any nucleus of the molecule and that it is relatively well localised in the molecular space.

The unambiguous characterisation of solid and molecular electrides is essential to distinguish them from other species that exhibit similar properties. In a recent work by some of us,[28] we characterised five molecular electrides using three different criteria that provide support to the presence of an isolated electron, namely: i) the existence of a non-nuclear attractor (NNA) of the electron density (also named quasiatoms in electrides)[20-22], that is a maximum on the electron density at points distinct from nuclear positions, ii) the presence of an electron localisation function (ELF) basin in the same region of the NNA, and iii) negative values of the Laplacian of the electron density ($\nabla^2\rho$) in the NNA. Our study also showed that the mere existence of NNAs with negative values of $\nabla^2\rho$ was enough to characterize an electride.[28] These criteria apply except when the NNAs are

located in the close vicinity of an atom because in this case the isolated nature of the electron is dubious.[28]

The term molecular cluster refers to a relatively small aggregation of atoms or molecules. Clusters are homo- or heteroatomic nanoparticles that behave as a link between the atom or the molecule and the bulk material, thus constituting an intermediate phase of matter.[29] They exhibit characteristics of both forms of matter (atom and bulk) and, consequently, they have specific properties that depend critically on their size and shape. Some clusters with closed-shell or same-spin half-filled electronic structure are particularly stable because they are aromatic.[30] This is the case of Li_3^+ or Li_4^{2+} that follow the $4n+2$ Hückel rule, [31],[32] the $B_{12}H_{12}^{2-}$ that obeys the $2n+2$ Wade-Mingos criterion,[33-34] the C_{60}^{10+} and C_{80}^{+8} that satisfy the $2(n+1)^2$ Hirsch formula[35] or the C_{60}^- (S=11/2) that fulfils the $2n^2+2n+1$ (with S=n+1/2) rule.[36] With this idea in mind, in a recent work some of us looked for aromatic molecular clusters with octahedral symmetry.[37] We analysed the aromatic character and chemical bonding of an extensive set of octahedral clusters O_h X_6^q (X = Li–C and Be–Si) with charges q going from −2 to +4 and in $^{2S+1}A_{1g}$ electronic states with spin multiplicities ranging from the singlet (S = 0) to the septet (S = 3). By serendipity, we found that among all of them O_h Li_6^+ (S=3/2) and Be_6 (S=2) exhibit a unique electronic structure that reminds that of the metals.[37] These systems have several NNAs and have all (or most of the) valence electrons located in these NNAs. Because these metal clusters exhibit similar typical characteristics of electrides (the presence of NNAs), we propose to name this particular class of electrides as *metal cluster electrides*. The main aim of this work is to report the molecular and electronic structure of excited-state Li_6^+ (S=3/2) and Be_6 (S=2) metal cluster electrides and to establish a computational

protocol that provides the means to characterize and design new compounds with metal cluster electride character.

Except otherwise stated, the results discussed below are obtained with the UB3LYP/aug-cc-pVTZ method. Spin contamination at this level of theory was found to be negligible for the two species studied. It is worth mentioning that we decided not to use the ELF to characterize the studied systems because there is not an unambiguous way to represent the ELF in open-shell species[38-42] like in the studied high-spin metal clusters. Instead, we use the negative values of the Laplacian of the electron density that provide a direct measure of the electron density accumulation in real space.[43-44]

Results and discussion

The results section is divided as follows: first, a description of the geometric and electronic structure of the abovementioned octahedral clusters in their ground and excited states is provided; second, the chemical bonding features of metal cluster electrides are discussed and compared with electrides; finally, the aromatic character of these clusters is studied in detail.

Li_6^+ with S=3/2 has a perfect octahedral symmetry with the Li–Li distance ranging from 3.006 to 3.156 Å for the different levels of theory we have used (see Table S1 of the SI). Our best estimate is the 3.087 Å obtained at the UCCSD/aug-cc-pVTZ level. Although the Li clusters are usually difficult to describe due to the diffuse nature of the valence electron and the multiconfigurational character of their wavefunctions,[45] $O_h(^4A_{1g})$ Li_6^+ is reasonably well described at the monoconfigurational level. Indeed, the T_1 test[46] at the UCCSD/aug-cc-pVTZ//QCISD/aug-cc-pVTZ level for this system gives 0.042, which is below the recommended threshold for open-shell species.[47] The five valence electrons

occupy the a_{1g} and t_{1u} molecular orbitals, the latter ones being half-filled with three same-spin electrons (see Figure 1a). Interestingly, the SOMO-LUMO energy gap for $O_h(^4A_{1g})$ Li_6^+ is significantly small (0.09 eV at the B3LYP/aug-cc-pVTZ level of theory). The three unpaired t_{1u} electrons provide what is called no-pair ferromagnetic bonding that has been extensively described for high-spin lithium clusters.[48] O_h Li_6^+ (S=3/2) is an excited state for the cationic hexamer of Li. The ground state for this species, which is 20.7 kcal/mol more stable at the UCCSD(T)/aug-cc-pVTZ//B3LYP/aug-cc-pVTZ level, is the $C_{2v}(^2A_1)$ state, whereas the $D_{2h}(^2B_{2u})$ is only 0.6 kcal/mol higher than the lowest in energy C_{2v} structure (see Table S3 in the SI). $C_{2v}(^2A_1)$ and $D_{2h}(^2B_{2u})$ are almost degenerate states with octahedral distorted geometries. Previous studies with the coupled-cluster method found the $C_{2v}(^2A_1)$ to be the ground state,[49-50] whereas MRD-CI calculations favoured the $D_{2h}(^2B_{2u})$ structure.[51] Lithium clusters are characterised by a flat potential energy surface that allows the molecule to easily sample a variety of geometries with different symmetries. For the $C_{2v}(^2A_1)$ state, the SOMO-LUMO energy gap is also small (0.06 eV with the B3LYP/aug-cc-pVTZ method).

We employed the Quantum Theory of Atoms-in-Molecules (QTAIM) analysis to characterize the chemical bonding and topological features of this compound. QTAIM of $O_h(^4A_{1g})$ Li_6^+ provides the picture shown in Figure 1b obtained with the UB3LYP/aug-cc-pVTZ method. The most significant result obtained from the topological analysis of the electron density of $O_h(^4A_{1g})$ Li_6^+ is the unusually high number of non-nuclear attractors (NNAs). As can be seen, this species has eight NNAs located in the faces of the octahedral structure. The presence of NNAs is not a frequent feature of molecular densities. As some of us have shown, NNAs are a

landmark feature of electrides.[28] Although NNAs are typically found in the interstitial regions of the Li clusters,[52] $O_h(^4A_{1g})$ Li_6^+ represents the first example of a lithium cluster with more NNAs than nuclei. Previous results on Li_2, Li_4, and Li_6 show that these clusters have 1, 2, and 3 NNAs respectively.[53-55] For the diatomic Li_2 molecule, the Li–Li distance at which these NNAs appear was found to be in the range 2.15–3.45 Å.[53] The Li–Li distance in $O_h(^4A_{1g})$ Li_6^+ is in between this range of distances. We checked the number of NNAs in $O_h(^4A_{1g})$ Li_6^+ with different functionals, correlated methods, and basis sets and in all cases we found that the number of NNAs was either 8 or 12 (see Table S1). In the latter case, the NNAs are located in the centre of the Li–Li edges of the octahedron. The change in the number of NNAs is not unexpected due to the extremely flat profile of the electron density in this species.[56] Our best estimate is provided by the UCCSD/aug-cc-pVTZ density that gives eight NNAs. To illustrate the important role of NNAs on the electronic structure of this species, the population of each NNA region has been calculated. The population of these NNAs at the UB3LYP/aug-cc-pVTZ level is 0.43 e^- and its degree of localisation is 22%. The NNA population is similar to the ones we previously found for molecular electrides (e.g. 0.53 e- for tetracyanoquinodimethane derivative, $TCNQLi_2$)[28] but the degree of localisation is lower (51% for $TCNQLi_2$), indicating a more delocalised situation in $O_h(^4A_{1g})$ Li_6^+ than in molecular electrides. Figure 1c plots an isosurface of $\nabla^2\rho$ showing the presence of regions of negative Laplacian of the electron density located around the NNAs. Negative values of $\nabla^2\rho$ indicate negative charge concentration.

One can also analyse the isosurfaces of the alpha and beta electrons contributions to the Laplacian of the electron density ($\nabla^2\rho_\alpha$ and $\nabla^2\rho_\beta$). Since the number of alpha valence electrons in this open-shell system (4 e-) is not equal to the number of the

beta ones (1 e-), different $\nabla^2\rho_\alpha$ and $\nabla^2\rho_\beta$ isosurfaces are expected (see Figure 1d). In O_h Li_6^+ (S=3/2), the alpha electrons are highly delocalised around NNAs, while the beta electron is even more delocalised and located in the centre of the octahedron. At high $\nabla^2\rho_\alpha$ isosurface values, one can distinguish twelve regions (situated between each pair of Li atoms) with significant electron density. However, the regions where the NNAs are located (face regions) are more delocalised than the edge regions. In fact, at the large negative values of the Laplacian, the Laplacian in the face regions is not visible and it is only present in the twelve edge regions (see Figure S6 of the SI). Interestingly, these findings show that the electron density in the NNAs is quite delocalised according to QTAIM analysis. On the other hand, for an isosurface of -0.002 a.u. one is able to distinguish a single region in the isosurface of $\nabla^2\rho_\beta$. However, at more negative isosurface values, this isosurface is bisected into twelve regions, the same number obtained from the $\nabla^2\rho_\alpha$ isosurface analysis. Remarkably, the beta region is more delocalised than the alpha ones (see Figure S6 of the SI).[57] Therefore, most valence electrons in O_h Li_6^+ (S=3/2) are located far from nuclei and are quite delocalised. The energetic cost of moving the valence electrons away from nuclei is offset by avoiding repulsive Pauli effects due to core electrons and by lowering the kinetic energy.[58-59] The delocalised nature of valence electrons points out the multicenter character of the bonding in $O_h(^4A_{1g})$ Li_6^+. Despite the presence of NNAs in O_h Li_6^+ (S=3/2), their electrons are clearly more delocalised than the NNA ones of electrides.

The map of the electrostatic potential (see Figure S1 in the SI) does not display areas of negative electrostatic potential close to the NNAs. However, despite recent claims,[60] we consider that the electrostatic potential is not a good tool to

characterize electrides and, in fact, we have found several examples in which electrostatic potential is not a good indicator of electride character.[28] Mainly, when regions with abundance of electrons such lone pairs are close to NNA regions, the former hinder the identification of the latter. Moreover, Dale and coworkers[7, 56] demonstrated that noncovalent interaction (NCI) plots are ideal to reveal the presence of confined electrons in solid electrides. These electrons are located in regions of low electron density with low reduced-gradient values and, consequently, they are disclosed in the NCI maps. Figure 1e plots one of these maps that show the presence of a green region indicating the existence of a weak attractive interaction between the interstitial regions around the NNAs position and the nuclei. The values of the isotropic static electronic polarizability ($\overline{\alpha^e}(0;0)$ = 308.1 a.u.) and of the second hyperpolarizability ($\gamma_{\|}{}^e(0;0,0,0)$ = 3.66x10^5 a.u.) are rather high for such a small molecule. These values are in line with the results obtained by some of us for molecular electrides,[4, 28] showing the potential electride character of this type of lithium clusters. For symmetry reasons, the value of the average first hyperpolarizability is zero.

Lithium clusters present a flat potential energy surface, thus, transitions between different geometries can be readily observed. NNAs are a key characteristic of these systems and have been directly related to the existence of electrides.[28] The question is whether these NNAs are stable along the potential energy surface of Li_6^+. To assess the presence of NNAs on the S=3/2 state of Li_6^+, we performed Car-Parrinello molecular dynamics (CPMD) of $O_h(^4A_{1g})$ Li_6^+ at 300 K and we observed that once the octahedral symmetry is lost, the number of NNAs decreases. The average number of NNAs found in a trajectory of 1.2 ps is 2.1 (see Figure S7 of the SI). In all analysed snapshots, we found at least 1 NNA. Interestingly, the valence

electron density is found to be quite delocalised when the number of NNAs is high, while is more localised when the number of NNAs is close to 1. The average percentage of localisation of these NNAs is 30%, 35%, 42.5%, and 68% for representative geometries with 4, 3, 2, and 1 NNAs, respectively (Figure S7). Therefore, at room temperature the system oscillates between highly delocalised and highly localised (electride) character depending on the geometry that the system adopts along the molecular dynamics trajectory.

As discussed in the previous paragraphs, the electronic configuration of $O_h(^4A_{1g})$ Li_6^+ is compatible with an aromatic molecule. In fact, with five valence electrons, this species for n = 1 follows the $2n^2+2n+1$ (S = n+1/2) rule[36] for open-shell spherical aromatic species. The NICS values in the centre of the octahedron and in the centre of the faces are –19.4 and –14.2 ppm, respectively, thus denoting a 3D aromatic species. The electronic multicentre index (MCI) for the six Li atoms is 0.068, almost identical to that of benzene (0.072 at the B3LYP/6-311++G(d,p) level)[61]. The shape of the Laplacian of the electron density and the metalloaromatic character[62-63] of this species prove the presence of delocalised electrons in the interstitial regions of the octahedron in the $O_h(^4A_{1g})$ Li_6^+ species. We were curious as to whether this electronic structure can result in strong ring currents, so we calculated the current density maps with the Coupled-perturbed Restricted Open-Shell Hartree-Fock (CROHF) method[64] with a cc-pVDZ basis set, using the ipsocentric model for the ring-current response[65-69] within the single-determinant approximation. Plots in Figure 2a represent the all-electron electronic linear response to a magnetic field oriented along the C_4 axis. A clockwise (counterclockwise) circulation corresponds to a paratropic (diatropic) current. In the Supporting information we provide the plots for the valence and

t_{1u} electrons with a magnetic field oriented along the C_4 and C_3 axes of the octahedron (Figure S2.1-S2.4, SI). Two main characteristics of the observed ring current are: (i) a delocalised diatropic "ring" current located within the polyhedron molecular volume where the overlap between radial-2p atomic functions is maximal, and (ii) a set of well-localised paratropic circulations centred about the nuclear sites. Inside the octahedron, a delocalised diatropic current is observed, fully originating from a $t_{1u} \rightarrow t_{2g}$ translationally allowed transition due to the top spin-up electrons in $O_h(^4A_{1g})$ Li_6^+. Besides that, on the planes containing either equatorial atoms or a triangular face, paratropic localised currents become an important feature of the maps. As evident from the decomposition into orbital currents, the top t_{1u} spin-up electrons play an important role in the description of these localised but somewhat weak currents in Li_6^+, due to the mixed paratropic $t_{1u} \rightarrow t_{1u}$ and diatropic $t_{1u} \rightarrow t_{2g}$ character of the current contribution from these electrons (see Figure S3 for a scheme of the relevant transitions).

Be_6 with S =2 has a perfect octahedral structure like $^4A_{1g}$ Li_6^+. The presence of 12 valence electrons instead of 5 in $^4A_{1g}$ Li_6^+ makes the bond stronger and the Be–Be distance shorter with values in between 2.037 and 2.092 Å for the different levels of theory we have used (see Table S1 of the SI). Our best estimate is the UCCSD/aug-cc-pVTZ value of 2.063 Å. At this level of theory, the T_1 test value of 0.016 shows that $^5A_{1g}$ Be_6 has monoconfigurational character. The highest-lying four valence electrons have the same spin and half-fill the a_{1g} and t_{2g} molecular orbitals (see Figure 3a) and the SOMO-LUMO energy gap is again significantly small (0.09 eV with the B3LYP/aug-cc-pVTZ method). Like for $^4A_{1g}$ Li_6^+, the $^5A_{1g}$

Be_6 state is an excited state of Be_6. With the UCCSD(T)/aug-cc-pVTZ//QCISD/aug-cc-pVTZ method, the ground state is the $D_{2h}(^1A_g)$ state. The $C_{2v}(^1A_1)$ is less stable by only 0.2 kcal/mol. With respect to the ground state, the $^5A_{1g}$ Be_6 state lies only 4.1 kcal/mol higher in energy (see Table S3 of the SI), indicating a flat potential energy surface. Be_6 is the first Be cluster the ground state of which is controversial.[70-71] Depending on the level of calculation used, different authors have pointed out the following ground states: $O_h(^5A_{1g})$,[72] $D_{3d}(^3A_{1g})$,[73-74] $C_{2v}(^1A_1)$,[73] $C_{2h}(^3A_u)$,[75] and $D_{2h}(^1A_g)$,[70, 73] although all CCSD calculations favour the D_{2h} ^1A_g state.[70, 73] Calculated enthalpies at 298 K locate the $^5A_{1g}$ Be_6 state at only 2.1 kcal/mol with respect to the $D_{2h}(^1A_g)$ ground state (Table S3). Hence, production of this cluster in collimated supersonic cluster beams cannot be discarded.

The UB3LYP/aug-cc-pVTZ QTAIM plot of $O_h(^5A_{1g})$ Be_6 electron density is given in Figure 3b. As in $O_h(^4A_{1g})$ Li_6^+, the total number of NNAs is significant (higher than the number of atoms) and depends on the level of calculation. In the case of $O_h(^5A_{1g})$ Be_6, the located NNAs are 12 or 20 depending on the level of theory used (see Table S1). At the UCCSD/aug-cc-pVTZ and UB3LYP/aug-cc-pVTZ levels of theory there are 20 NNAs. For Be_2, the Be–Be distance at which these NNAs appear is more narrow than in Li_2 (2.36–2.45 Å).[53] The Be–Be distance in $^5A_{1g}$ Be_6 is somewhat shorter. The population of these NNAs at the UB3LYP/aug-cc-pVTZ level is only 0.01 e^- for the NNAs in the faces and 0.51 e^- for the NNAs of the edges. The latter have a degree of localisation of 17%. These values are similar to the ones obtained for Li_6^+ (see above). The isosurface of $\nabla^2\rho$ depicted in Figure 3c indicates the presence of regions of negative Laplacian of the electron density located around the NNAs. Generally, the isosurface of $\nabla^2\rho_\alpha$ is quite similar to that

of the $O_h(^4A_{1g})$ Li_6^+ species. Yet, the only difference between the two metal clusters is the positioning of the isosurface of $\nabla^2\rho_\alpha$, which in the case of $O_h(^5A_{1g})$ Be_6 is more displaced out of the centre of the octahedral structure. The $\nabla^2\rho_\beta$ isosurface is analogous to $\nabla^2\rho_\alpha$ and they only slightly differ in the location of the isosurface. From the $\nabla^2\rho_\alpha$ and $\nabla^2\rho_\beta$ isosurfaces for $O_h(^5A_{1g})$ Be_6, one can distinguish twelve regions which coincide on the position of the 12 NNAs that are located in the edges. Regarding the regions where the 8 faced NNAs are situated, a localised surface is not found because actually they are less localised than the bonded NNAs regions (see Figure S6 of the SI). In fact, the previous result is not unexpected because, according to QTAIM, the faced NNAs are more delocalised than the ones in the edges.

As for $O_h(^4A_{1g})$ Li_6^+, the electrostatic potential plot does not show areas of negative electrostatic potential close to the NNAs (see Figure S1 in the SI). Figure 3e plots the NCI map for $O_h(^5A_{1g})$ Be_6 that shows a blue region due to the presence of an attractive interaction between the interstitial regions around the NNAs position and the Be atoms. The values of the isotropic static electronic polarizability ($\overline{\alpha^e}(0;0)$ = 157.9 a.u.) and of the second hyperpolarizability ($\gamma_{\|}{}^e(0;0,0,0)$ = $2.85\text{x}10^5$ a.u.) are somewhat smaller than those found for $O_h(^4A_{1g})$ Li_6^+. All indicators of aromaticity point out that the aromaticity of $O_h(^5A_{1g})$ Be_6 is higher than that of $O_h(^4A_{1g})$ Li_6^+. Indeed, NICS values in the centre of the octahedron and in the centre of the faces are –31.2 and –15.3 ppm, respectively. The MCI for the three Be atoms forming a face of the octahedron is 0.158 e^- and for the six Be atoms is 0.080 e^-. The current density maps obtained with the CROHF/cc-pVDZ method (see Figure 3b) show similar currents in $O_h(^5A_{1g})$ Be_6 and $O_h(^4A_{1g})$ Li_6^+, the former being more intense. Again the main diamagnetic transition corresponds to the t_{1u}

→ t_{2g} transition that in $O_h(^5A_{1g})$ Be_6 is strengthened by the small energy gap between these orbitals (see Figure S3).

As a whole, we have identified two O_h species ($^4A_{1g}$ Li_6^+ and $^5A_{1g}$ Be_6) with a large number of NNAs and with all or almost all valence electrons located in these NNAs. The chemical bonding in these molecules is neither classical covalent nor ionic. In fact, the chemical bonding of these molecules reminds that of solid metals[54] where the array of metal cations is surrounded by a "sea" of valence electrons (electron-sea model). Consequently, we suggest that these species could be used as molecular models for the study of the metal bonding in finite systems. The presence of high delocalised NNAs or quasiatoms and delocalised regions provided by the negative values of the Laplacian of the electron density indicate that we are dealing with a new type of electrides that have delocalised polyattractor character.

Methods

Most of the calculations were performed with the Gaussian 09 package[76] by using the B3LYP[77-79] hybrid density functional and the aug-cc-pVTZ basis set.[80-81] In some cases, we also used other density functionals (BP86, M06-2X) and correlated methods (MP2, QCISD, CCSD(T)) with a variety of Dunning and Pople basis sets. The unrestricted formalism was used for all calculations. The geometry optimisations were performed without symmetry constraints, and analytical Hessians were computed to confirm that the optimised structures are indeed minima (zero imaginary frequencies). Aromaticity was evaluated by means of multicentre indices (MCI),[82-83] nucleus-independent chemical shifts (NICS),[84] and the calculation of ring currents.[64-65, 85] The QTAIM analysis was carried out

with the AIMPAC collection of programs,[86] the localisation (LI), delocalisation (DI), and MCI indices were obtained with the ESI-3D program,[87-88] the NCI (Noncovalent Interactions) maps were generated with the NCIPLOT program,[89] and the ring currents with the SYSMO quantum chemistry code.[90] More details on the method of calculation can be found in the Supplementary Information.

Acknowledgements

This work has been supported by the Ministerio de Economía y Competitividad (MINECO) of Spain (Projects CTQ2017-85341-P to M.S., CTQ2014-52525-P to E.M. and J.M.L. and EUIN2017-88605 to E.M., and grant No. BES-2012-052801 to V.P.), the Basque Government (Project IT588-13), and the Generalitat de Catalunya (Project 2017SGR39, Xarxa de Referència en Química Teòrica i Computacional, ICREA Academia 2014 prize for M.S., and grant No. 2014FI_B 00429 to O.E.B.). M.G.-B. thanks the Ramón Areces Foundation for a postdoctoral fellowship. F.F. acknowledges financial support of the Beatriu de Pinós programme from AGAUR for the postdoctoral grant BP_A_00339 and BP_A2_00022. The EU under the FEDER grant UNGI10-4E-801 (European Fund for Regional Development) has also funded this research.

Keywords: metal cluster electrides · electrides · multicentric bonding · metalloaromaticity · ring currents · electronic structure

Supplementary Information

A detailed description of the computational method used, Cartesian coordinates of all optimised structures. Tables with geometries and number of NNAs for several methods and basis sets used. Figures with electrostatic potentials, current densities, and NCI and ELF plots. Tables with relative energies of isomers and localisation and delocalisation indices.

References

[1] J. L. Dye, M. Y. Redko, R. H. Huang and J. E. Jackson in *Role of Cation Complexants in the Synthesis of Alkalides and Electrides*, *Vol. 59* Eds.: E. Rudi van and B.-J. Kristin), Academic Press, **2006**, pp. 205-231.
[2] J. L. Dye, *Acc. Chem. Res.* **2009**, *42*, 1564-1572.
[3] B. G. Janesko, G. Scalmani and M. J. Frisch, *J. Chem. Theory Comput.* **2016**, *12*, 79-91.
[4] M. Garcia-Borràs, M. Solà, J. M. Luis and B. Kirtman, *J. Chem. Theory Comput.* **2012**, *8*, 2688-2697.
[5] H.-M. He, Y. Li, W.-M. Sun, J.-J. Wang, D. Wu, R.-L. Zhong, Z.-J. Zhou and Z.-R. Li, *Dalton Trans.* **2016**, *45*, 2656-2665.
[6] H.-M. He, Y. Li, H. Yang, D. Yu, D. Wu, R.-L. Zhong, Z.-J. Zhou and Z.-R. Li, *J. Phys. Chem. C* **2017**, *121*, 25531-25540.
[7] S. G. Dale and E. R. Johnson, *Phys. Chem. Chem. Phys.* **2016**, *18*, 27326-27335.
[8] M. Miyakawa, S. W. Kim, M. Hirano, Y. Kohama, H. Kawaji, T. Atake, H. Ikegami, K. Kono and H. Hosono, *J. Am. Chem. Soc.* **2007**, *129*, 7270-7271.
[9] M. Kitano, Y. Inoue, Y. Yamazaki, F. Hayashi, S. Kanbara, S. Matsuishi, T. Yokoyama, S.-W. Kim, M. Hara and H. Hosono, *Nat. Chem.* **2012**, *4*, 934-940.
[10] M. Kitano, S. Kanbara, Y. Inoue, N. Kuganathan, P. V. Sushko, T. Yokoyama, M. Hara and H. Hosono, *Nat. Commun.* **2015**, *6*, 6731.
[11] Y. Inoue, M. Kitano, K. Kishida, H. Abe, Y. Niwa, M. Sasase, Y. Fujita, H. Ishikawa, T. Yokoyama, M. Hara and H. Hosono, *ACS Catalysis* **2016**, *6*, 7577-7584.
[12] M. Hara, M. Kitano and H. Hosono, *ACS Catalysis* **2017**, *7*, 2313-2324.
[13] J. Wu, Y. Gong, T. Inoshita, D. C. Fredrickson, J. Wang, Y. Lu, M. Kitano and H. Hosono, *Adv. Mater.* **2017**, *29*, 1700924.
[14] M. Kitano, Y. Inoue, M. Sasase, K. Kishida, Y. Kobayashi, K. Nishiyama, T. Tada, S. Kawamura, T. Yokoyama, M. Hara and H. Hosono, *Angew. Chem. Int. Ed.* **2018**, *57*, 2648-2652.
[15] S. Matsuishi, Y. Toda, M. Miyakawa, K. Hayashi, T. Kamiya, M. Hirano, I. Tanaka and H. Hosono, *Science* **2003**, *301*, 626-629.
[16] M. Y. Redko, J. E. Jackson, R. H. Huang and J. L. Dye, *J. Am. Chem. Soc.* **2005**, *127*, 12416-12422.
[17] K. Lee, S. W. Kim, Y. Toda, S. Matsuishi and H. Hosono, *Nature* **2013**, *494*, 336-340.
[18] S. Zhao, E. Kan and Z. Li, *WIREs: Comput. Mol. Sci.* **2016**, *6*, 430-440.
[19] H. Mizoguchi, M. Okunaka, M. Kitano, S. Matsuishi, T. Yokoyama and H. Hosono, *Inorg. Chem.* **2016**, *55*, 8833-8838.
[20] M.-S. Miao and R. Hoffmann, *Acc. Chem. Res.* **2014**, *47*, 1311-1317.
[21] M.-S. Miao and R. Hoffmann, *J. Am. Chem. Soc.* **2015**, *137*, 3631-3637.
[22] M.-S. Miao, R. Hoffmann, J. Botana, I. I. Naumov and R. J. Hemley, *Angew. Chem. Int. Ed.* **2017**, *56*, 972-975.
[23] M. Gatti, I. V. Tokatly and A. Rubio, *Phys. Rev. Lett.* **2010**, *104*, 216404.
[24] M. Marqués, G. J. Ackland, L. F. Lundegaard, G. Stinton, R. J. Nelmes, M. I. McMahon and J. Contreras-García, *Phys. Rev. Lett.* **2009**, *103*, 115501.
[25] M. Marqués, M. I. McMahon, E. Gregoryanz, M. Hanfland, C. L. Guillaume, C. J. Pickard, G. J. Ackland and R. J. Nelmes, *Phys. Rev. Lett.* **2011**, *106*, 095502.
[26] B. Silvi, *Struct. Chem.* **2017**, *28*, 1389-1397.

[27] X. Dong, A. R. Oganov, A. F. Goncharov, E. Stavrou, S. Lobanov, G. Saleh, G.-R. Qian, Q. Zhu, C. Gatti, V. L. Deringer, R. Dronskowski, X.-F. Zhou, V. B. Prakapenka, Z. Konôpková, I. A. Popov, A. I. Boldyrev and H.-T. Wang, *Nat. Chem.* **2017**, *9*, 440-445.
[28] V. Postils, M. Garcia-Borràs, M. Solà, J. M. Luis and E. Matito, *Chem. Commun.* **2015**, *51*, 4865-4868.
[29] R. L. Johnston, *Atomic and Molecular Clusters*, (Ed. D. S. Betts), Taylor & Francis, New York, **2002**.
[30] Z. Chen, S. Neukermans, X. Wang, E. Janssens, Z. Zhou, R. E. Silverans, R. B. King, P. v. R. Schleyer and P. Lievens, *J. Am. Chem. Soc.* **2006**, *128*, 12829-12834.
[31] A. N. Alexandrova and A. I. Boldyrev, *J. Phys. Chem. A* **2003**, *107*, 554-560.
[32] E. Hückel, *Z. Elektrochemie* **1937**, *43*, 752-788, 827-849.
[33] K. Wade, *J. Chem. Soc. D: Chem. Commun.* **1971**, 792-793.
[34] D. M. P. Mingos, *Acc. Chem. Res.* **1984**, *17*, 311-319.
[35] A. Hirsch, Z. Chen and H. Jiao, *Angew. Chem. Int. Ed.* **2000**, *39*, 3915-3917.
[36] J. Poater and M. Solà, *Chem. Commun.* **2011**, *47*, 11647-11649.
[37] O. El Bakouri, M. Duran, J. Poater, F. Feixas and M. Solà, *Phys. Chem. Chem. Phys.* **2016**, *18*, 11700-11706.
[38] A. D. Becke and K. E. Edgecombe, *J. Chem. Phys.* **1990**, *92*, 5397-5403.
[39] M. Kohout and A. Savin, *Int. J. Quantum Chem.* **1996**, *60*, 875-882.
[40] J. Melin and P. Fuentealba, *Int. J. Quantum Chem.* **2003**, *92*, 381-390.
[41] J. Pilmé, *J. Comput. Chem.* **2017**, *38*, 204-210.
[42] B. Silvi, *J. Phys. Chem. A* **2003**, *107*, 3081-3085.
[43] R. F. W. Bader, *Atoms in Molecules: A Quantum Theory*, Clarendon, Oxford, **1990**.
[44] R. F. W. Bader, *Chem. Rev.* **1991**, *91*, 893-928.
[45] A. N. Alexandrova, A. I. Boldyrev, X. Li, H. W. Sarkas, J. H. Hendricks, S. T. Arnold and K. H. Bowen, *J. Chem. Phys.* **2011**, *134*, 044322.
[46] T. J. Lee and P. R. Taylor, *Int. J. Quantum Chem., Quant. Chem. Symp.* **1989**, *S23*, 199-207.
[47] J. C. Rienstra-Kiracofe, W. D. Allen and H. F. Schaefer III, *J. Phys. Chem. A* **2000**, *104*, 9823-9840.
[48] D. Danovich and S. Shaik, *Acc. Chem. Res.* **2014**, *47*, 417-426.
[49] B. Temelso and C. D. Sherrill, *J. Chem. Phys.* **2005**, *122*, 064315.
[50] A. N. Alexandrova and A. I. Boldyrev, *J. Chem. Theory Comput.* **2005**, *1*, 566-580.
[51] I. Boustani, W. Pewestorf, P. Fantucci, V. Bonaić-Koutecký and J. Koutecký, *Phys. Rev. B* **1987**, *35*, 9437-9450.
[52] B. Silvi and C. Gatti, *J. Phys. Chem. A* **2000**, *104*, 947-953.
[53] A. Martín Pendás, M. A. Blanco, A. Costales, P. Mori Sánchez and V. Luaña, *Phys. Rev. Lett.* **1999**, *83*, 1930-1933.
[54] W. C. Cao, C. Gatti, P. J. McDougall and R. F. W. Bader, *Chem. Phys. Lett.* **1987**, *141*, 380-385.
[55] C. Gatti, P. Fantucci and G. Pacchioni, *Theor. Chim. Acta* **1987**, *72*, 433-458.
[56] S. G. Dale, A. Otero-de-la-Roza and E. R. Johnson, *Phys. Chem. Chem. Phys.* **2014**, *16*, 14584-14593.
[57] R. Rousseau and D. Marx, *Chem. Eur. J.* **2000**, *6*, 2982-2993.
[58] D. J. Singh, H. Krakauer, C. Haas and W. E. Pickett, *Nature* **1993**, *365*, 39-42.
[59] J. B. Neaton and N. W. Ashcroft, *Nature* **1999**, *400*, 141-144.

[60] A. Kumar and S. R. Gadre, *Phys. Chem. Chem. Phys.* **2015**, *17*, 15030-15035.
[61] F. Feixas, E. Matito, J. Poater and M. Solà, *J. Phys. Chem. A* **2007**, *111*, 4513-4521.
[62] F. Feixas, E. Matito, J. Poater and M. Solà, *WIREs: Comput. Mol. Sci.* **2013**, *3*, 105-122.
[63] A. I. Boldyrev and L.-S. Wang, *Chem. Rev.* **2005**, *105*, 3716-3757.
[64] A. Soncini, *J. Chem. Theory Comput.* **2007**, *3*, 2243-2257.
[65] T. A. Keith and R. F. W. Bader, *Chem. Phys. Lett.* **1993**, *210*, 223-231.
[66] S. Coriani, P. Lazzeretti, M. Malagoli and R. Zanasi, *Theor. Chim. Acta* **1994**, *89*, 181-192.
[67] E. Steiner and P. W. Fowler, *J. Phys. Chem. A* **2001**, *105*, 9553-9562.
[68] E. Steiner and P. W. Fowler, *Chem. Commun.* **2001**, 2220-2221.
[69] A. Soncini and P. W. Fowler, *Chem. Eur. J.* **2013**, *19*, 1740-1746.
[70] Š. Martin, L. Daniel, K. Martin, P. Michal, Č. Ivan and N. Pavel, *J. Phys. B: At. Mol. Opt. Phys.* **2012**, *45*, 085102.
[71] M. C. Heaven, J. M. Merritt and V. E. Bondybey, *Annu. Rev. Phys. Chem.* **2011**, *62*, 375-393.
[72] S. Srinivas and J. Jellinek, *J. Chem. Phys.* **2004**, *121*, 7243-7252.
[73] Y. Zhao, N. Li, W. G. Xu and Q. S. Li, *Int. J. Quantum Chem.* **2007**, *107*, 81-91.
[74] M. K. Beyer, L. A. Kaledin, A. L. Kaledin, M. C. Heaven and V. E. Bondybey, *Chem. Phys.* **2000**, *262*, 15-23.
[75] A. N. Alexandrova, A. I. Boldyrev, H.-J. Zhai, L.-S. Wang, E. Steiner and P. W. Fowler, *J. Phys. Chem. A* **2003**, *107*, 1359-1369.
[76] Gaussian 09, rev. A.02, M. J. Frisch, G. W. Trucks, H. B. Schlegel, G. E. Scuseria, M. A. Robb, J. R. Cheeseman, G. Scalmani, V. Barone, B. Mennucci, G. A. Petersson, H. Nakatsuji, M. Caricato, X. Li, H. P. Hratchian, A. F. Izmaylov, J. Bloino, G. Zheng, J. L. Sonnenberg, M. Hada, M. Ehara, K. Toyota, R. Fukuda, J. Hasegawa, M. Ishida, T. Nakajima, Y. Honda, O. Kitao, H. Nakai, T. Vreven, J. A. Montgomery Jr., J. E. Peralta, F. Ogliaro, M. Bearpark, J. J. Heyd, E. Brothers, K. N. Kudin, V. N. Staroverov, R. Kobayashi, J. Normand, K. Raghavachari, A. Rendell, J. C. Burant, S. S. Iyengar, J. Tomasi, M. Cossi, N. Rega, J. M. Millam, M. Klene, J. E. Knox, J. B. Cross, V. Bakken, C. Adamo, J. Jaramillo, R. Gomperts, R. E. Stratmann, O. Yazyev, A. J. Austin, R. Cammi, C. Pomelli, J. W. Ochterski, R. L. Martin, K. Morokuma, V. G. Zakrzewski, G. A. Voth, P. Salvador, J. J. Dannenberg, S. Dapprich, A. D. Daniels, Ö. Farkas, J. B. Foresman, J. V. Ortiz, J. Cioslowski and D. J. Fox, Gaussian, Inc., Pittsburgh, PA, **2009**.
[77] A. D. Becke, *J. Chem. Phys.* **1993**, *98*, 5648-5652.
[78] C. Lee, W. Yang and R. G. Parr, *Phys. Rev. B* **1988**, *37*, 785-789.
[79] P. J. Stephens, F. J. Devlin, C. F. Chabalowski and M. J. Frisch, *J. Phys. Chem.* **1994**, *98*, 11623-11627.
[80] T. H. Dunning Jr., *J. Chem. Phys.* **1989**, *90*, 1007-1023.
[81] R. A. Kendall, T. H. Dunning Jr. and R. J. Harrison, *J. Chem. Phys.* **1992**, *96*, 6796-6806.
[82] P. Bultinck, R. Ponec and S. Van Damme, *J. Phys. Org. Chem.* **2005**, *18*, 706-718.
[83] F. Feixas, E. Matito, J. Poater and M. Solà, *Chem. Soc. Rev.* **2015**, *44*, 6434–6451.
[84] P. v. R. Schleyer, C. Maerker, A. Dransfeld, H. Jiao and N. J. R. van Eikema Hommes, *J. Am. Chem. Soc.* **1996**, *118*, 6317-6318.
[85] S. Coriani, P. Lazzeretti, M. Malagoli and R. Zanasi, *Theor. Chim. Acta* **1994**, *89*, 181-192.

[86] F. W. Biegler-König, R. F. W. Bader and T.-H. Tang, *J. Comput. Chem.* **1982**, *3*, 317-328 (http://www.chemistry.mcmaster.ca/aimpac/).
[87] E. Matito, M. Duran and M. Solà, *J. Chem. Phys.* **2005**, *122*, 014109, Erratum, *íbid.*, **2006**, *125*, 059901.
[88] E. Matito in *ESI-3D: Electron Sharing Indexes Program for 3D Molecular Space Partitioning,* (http://iqc.udg.es/~eduard/ESI), Institute of Computational Chemistry and Catalysis, Girona, **2006**.
[89] J. Contreras-García, E. R. Johnson, S. Keinan, R. Chaudret, J.-P. Piquemal, D. N. Beratan and W. Yang, *J. Chem. Theory Comput.* **2011**, *7*, 625-632.
[90] P. Lazzeretti and R. Zanasi in *SYSMO package*. Additional routines by P. W. Fowler, E. Steiner, R. W. A. Havenith, and A. Soncini, University of Modena, **1980**.

Figure 1. $^4A_{1g}$ Li_6^+ (S=3/2) a) Schematic molecular orbital energy levels (energies in eV). b) Location of NNA (in yellow) obtained by QTAIM analysis. c) Laplacian of the electron density ($\nabla^2\rho$, isosurface is -0.0005 a.u.). d) Laplacian of the alpha and beta electron density ($\nabla^2\rho_\alpha$ and $\nabla^2\rho_\beta$ isosurfaces of -0.00214 a.u. in gray and blue, respectively). e) Noncovalent interactions (NCI, isosurface of 0.2). All reported data obtained at the UB3LYP/aug-cc-pVTZ level of theory.

a)

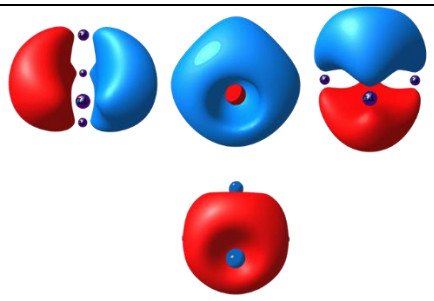

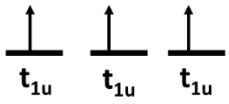

-0.268

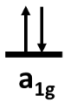

-0.353

b)

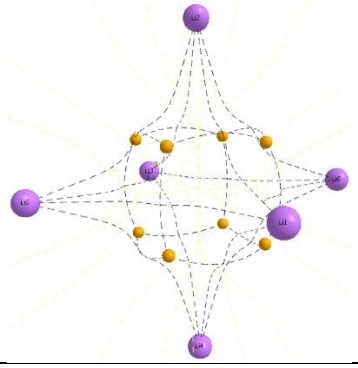

c)

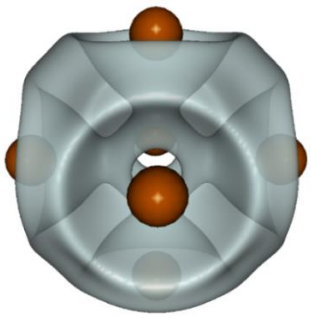

d)

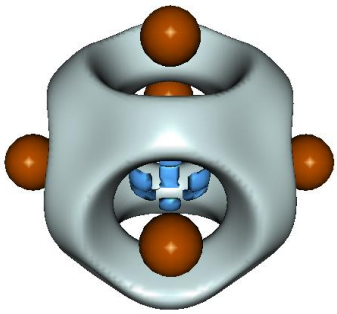

e)

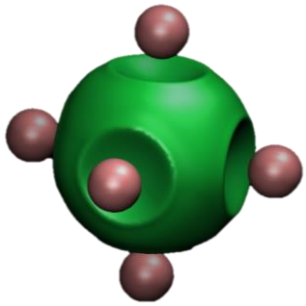

Figure 2. Magnetic field along C_4. Contributions to a) $^4A_{1g}$ Li_6^+ (S=3/2) and b) $^5A_{1g}$ Be_6 (S=2) current densities of all electrons (top) in a plane containing the four equatorial atoms.

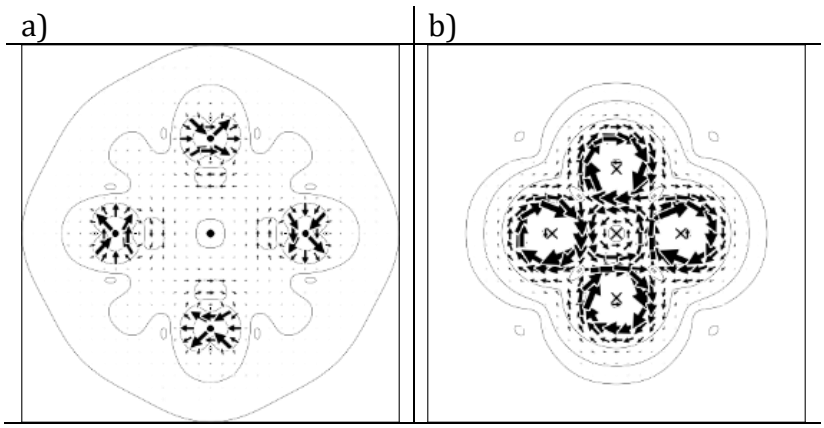

Figure 3. $^5A_{1g}$ Be_6 (S=2) a) Schematic molecular orbital energy levels (energies in eV). b) Location of NNAs (in yellow) obtained by QTAIM analysis. c) Laplacian of the electron density ($\nabla^2\rho$, isosurface in -0.0005 a.u.). d) Laplacian of the alpha and beta electron density ($\nabla^2\rho_\alpha$ and $\nabla^2\rho_\beta$ isosurfaces of -0.019 a.u. in gray and blue, respectively). e) Noncovalent interactions (NCI, isosurface of 0.2). All reported data obtained at the UB3LYP/aug-cc-pVTZ level of theory.

a)

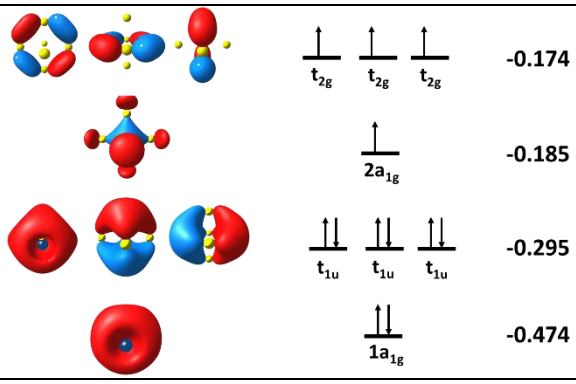

b)

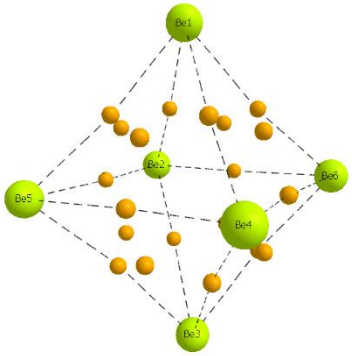

c)

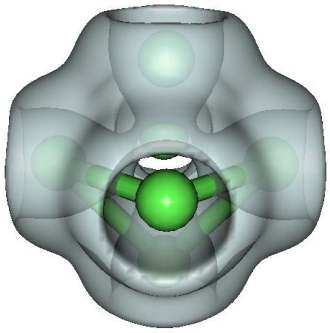

d)

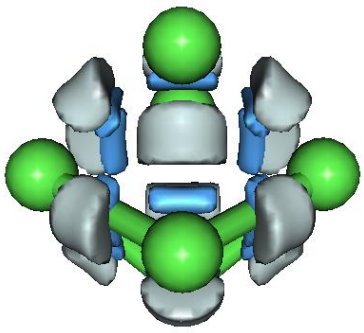

-0.019

e)

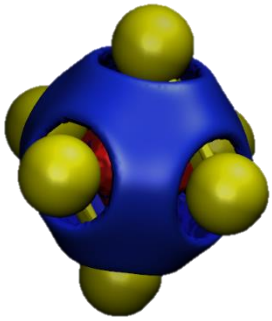

TABLE OF CONTENTS GRAPHIC

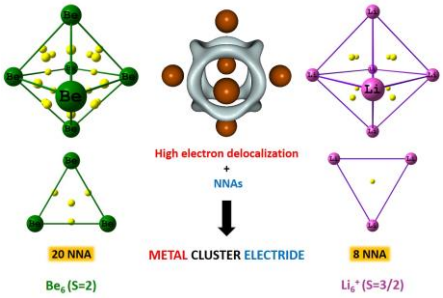

Metal cluster electrides are a new class of electrides with a larger number of non-nuclear attractors (NNAs) and with most of the valence electrons located in these NNAs. The chemical bond in these species reminds that of metallic crystals. Octahedral Li_6^+ (S=3/2) and Be_6 (S = 2) are reported to belong to this new class of electrides.